Title

Beneficial Effects of Kaempferol after Developmental Traumatic Brain Injury Is through Protection of Mitochondrial Function, Oxidative Metabolism, and Neural Viability

Journal

Journal of Neurotrauma, 36(8)

ISSN

0897-7151

Authors

Chitturi, Jyothsna
Santhakumar, Vijayalakshmi
Kannurpatti, Sridhar S

Publication Date

2019-04-15

DOI

10.1089/neu.2018.6100

Peer reviewed

JOURNAL OF NEUROTRAUMA 36:1264–1278 (April 15, 2019)

DOI: 10.1089/neu.2018.6100

Beneficial Effects of Kaempferol after Developmental Traumatic Brain Injury Is through Protection of Mitochondrial Function, Oxidative Metabolism, and Neural Viability

Jyothsna Chitturi,[1] Vijayalakshmi Santhakumar,[2,3] and Sridhar S. Kannurpatti[1]

Abstract

Oxidative energy metabolism is depressed after mild/moderate traumatic brain injury (TBI) during early development, accompanied by behavioral debilitation and secondary neuronal death. A TBI metabolome analysis revealed broad effects with a striking impact on energy metabolism. Our studies on mitochondrial modulators and their effects on brain function have shown that kaempferol, a stimulator of the mitochondrial Ca^{2+} uniporter channel (mCU), enhanced neural and neurovascular activity in the normal brain and improved stimulus-induced brain activation and behavior after TBI during early development. Because kaempferol enhances mitochondrial Ca^{2+} uptake and cycling, with protective effects after TBI, we tested the hypothesis that kaempferol treatment during the acute/subacute stage after TBI (0–72 h) acted on mitochondria in improving TBI outcome. Developmental age rats (P31) underwent TBI and were treated with vehicle or kaempferol (1 mg/kg intraperitoneally) in three doses at 1, 24, and 48 h after TBI. Brains were harvested at 72 h and subjected to liquid chromatography mass spectrometric measurements. Decrease in pyruvate and tricarboxylic acid (TCA) cycle flux were observed in the untreated and vehicle-treated group, consistent with previously established energy metabolic decline after TBI. Kaempferol improved TCA cycle flux, maintained mitochondrial functional integrity as observed by decreased acyl carnitines, improved neural viability as evidenced by higher N-acetyl aspartate levels. The positive outcomes of kaempferol on metabolic profile corresponded with improved sensorimotor behavior.

Keywords: calcium uniporter; dietary flavonoid; kaempferol; metabolomics; mitochondrial; N-acetyl aspartate; oxidative metabolism; pediatric; traumatic brain injury

Introduction

Developmental differences in children between two and nine years such as excitatory neurotransmission,[1–3] higher neurometabolic rates,[4] higher neural cell numbers,[5] increased myelination,[6,7] and different neurovascular activity compared with adults,[1,3,8,9] constitute a unique neurophysiological phase. These age-dependent features contribute to distinct neuropathological consequences of traumatic brain injury (TBI) to the developing brain. Because depressed energy levels exacerbate secondary neurodegeneration,[10] rescuing brain energy metabolism after TBI at all ages is crucial. It will have a greater impact on the developing brain, however, by rescuing several ongoing energy dependent developmental plasticity processes.

Previous studies have characterized the acute/subacute stage of the developmental rat model of TBI and observed a transient energy metabolic depression between 0 and 48 h that recovered thereafter.[11–15] Our recent metabolomic studies showed metabolic depression even at 72 h after developmental TBI, impinging on neural viability and subsequent neurodegeneration.[16] Because chronic studies suggest prolonged energy metabolic deficits after TBI,[17] it is highly likely that a large pool of surviving neural populations may carry long-term mitochondrial functional deficits. Supporting this view, previous studies have shown differential impact of TBI on mitochondria in various brain regions.[18]

Mitochondria are currently considered to play an active role in cellular signaling in addition to their traditional role as energy producing organelles. Mitochondrial energy metabolism and neural signaling are dynamically coupled through the mitochondrial Ca^{2+} uptake and efflux process via the mitochondrial Ca^{2+} uniporter channel (mCU).[19] Thus, metabolic deficits accompanying TBI via mitochondrial dysfunction additionally can affect neural signaling and hence brain circuit function.

In this regard, it is well known that mechanically injured areas of the brain attract and increase the frequency of cortical spreading depression (CSD).[20] Hence, early-stage therapeutic strategies that maintain baseline energy metabolism and spontaneous neural activity of cellular populations can be protective against adverse

Departments of [1]Radiology and [2]Pharmacology, Physiology & Neuroscience, Rutgers New Jersey Medical School, Newark, New Jersey.
[3]Molecular, Cell and Systems Biology, University of California Riverside, Riverside, California.

neurological outcomes after TBI. Because of the critical role of mitochondria in coupling brain oxidative energy metabolism and neural signaling activity,[19,21–25] and because mitochondrial degeneration has been identified in the neural, astrocytic, and vascular compartments after TBI,[18,26] mitochondria are suitable therapeutic targets in the TBI pathological process.

Our *in vivo* imaging studies on mitochondrial modulators and their effects on brain function indicated that kaempferol, a stimulator of the mitochondrial Ca^{2+} uniporter channel (mCU), enhanced spontaneous/stimulus-evoked neural activity and neurovascular responses in the normal brain.[24,25] In a pre-clinical rat model of TBI, treatment with intraperitoneal kaempferol (1 mg/kg) during the acute/subacute stage (0–72 h after TBI) in three doses separated by 24 h, significantly improved the long-term behavioral and brain function assessed two months post-TBI.[27]

We hypothesized that the protective action of kaempferol after TBI was through a mitochondrial mechanism of action. Based on the broad metabolomic impact of developmental TBI determined previously,[16] we examined the effects of kaempferol treatment on the TBI metabolome to test the mechanism of action of kaempferol. Metabolomic changes were determined by an untargeted multivariate analysis of a broad range of metabolites (197 metabolites) identified by liquid chromatography mass spectrometry (LC/MS) of the brain extracts at 72 h after TBI. N-acetyl aspartate (NAA), a neuronal marker, was used as a correlate of neural viability.[28,29] Metabolomic changes were correlated with TBI-induced sensorimotor behavioral outcomes.

Methods

Animals

Male Sprague-Dawley rats (23–24 days old; weighing 60–80 g) were procured from Charles River Laboratories, Wilmington, MA, and housed under controlled conditions. All procedures were approved by the Institutional Animal Care and Use Committee of Rutgers Biomedical and Health Sciences-New Jersey Medical School in accordance with the National Institutes of Health policy on the use of research animals. Blinding of animal groups for behavior was not performed because the same personnel performing surgical and injury procedures also performed the behavioral tests.

Lateral fluid-percussion injury

Animals underwent a lateral fluid percussion injury (FPI) aged P31 (Fig. 1A) in a similar manner to our previous studies and those of other independent groups[30,31] and were assigned randomly for the various treatments. For Luer lock placement, rats were anesthetized with intraperitoneal ketamine (80 mg/kg)-xylazine (10 mg/kg) and positioned on a stereotaxic frame. After ascertaining surgical plane anesthesia by the absence of tail-pinch reflexes, a 3 mm craniotomy was performed on the left side of the skull −5 mm posterior to the bregma and 3 mm lateral to the sagittal suture keeping the dura intact. A Luer lock syringe hub was glued surrounding the exposed dura using a cyanoacrylate adhesive. The TBI was performed 24 h after Luer lock implantation.

Rats were anesthetized with 2% isoflurane in an induction chamber, observed for anesthesia mediated loss of consciousness through head tilt, and transferred quickly to the FPI device (Virginia Commonwealth University, Richmond, VA). The Luer lock hub was affixed to the syringe of the FPI device under isoflurane anesthesia. A pendulum drop delivered a brief 20 msec impact on the intact dura. The impact pressure was measured by an extracranial transducer and controlled between 1.8–2.0 atm. Overall duration under isoflurane anesthesia and the FPI procedure was approximately 2–3 min. After injury, rats were transferred to a soft bedding cage and monitored for the return of righting reflex and any signs of seizures for the next 30 min. No special temperature management was necessary.

A mortality rate of 10% (4 of 36 animals) was observed throughout the current study. Two naive animals were lost—one immediately after ketamine administration and another during the Luer lock implantation procedure. Two TBI animals were lost—one at 24 h after the first dose of kaempferol treatment and another at 24 h after first vehicle dose. The 32 surviving animals were included in the study after randomly grouping into sham ($n=6$), TBI-untreated ($n=9$), TBI+ vehicle ($n=7$), and TBI+ kaempferol ($n=10$). Sham and TBI-untreated animal subjects from our previously published study[16] were combined with additional new animal subjects in the current study to achieve adequate sample sizes. Animals were monitored within their cage environment daily throughout the duration of the experiments.

Tissue sample extraction and liquid chromatography/mass spectrometry (LC/MS)

At 72 h after TBI (Fig. 1A), animals were decapitated and brains rapidly removed (<60 sec). Cerebellum and brain stem areas were removed, cerebral hemispheres separated (Fig. 1B; schematic), and snap frozen in liquid nitrogen and stored at −80°C. Brain tissue samples were weighed and disrupted in extraction buffer (80% methanol in water) using a microhomogenizer. Each sample was transferred to a pre-cooled (dry ice) homogenization tube with 4 mL of pre-cooled 80% methanol and homogenized for 15 sec

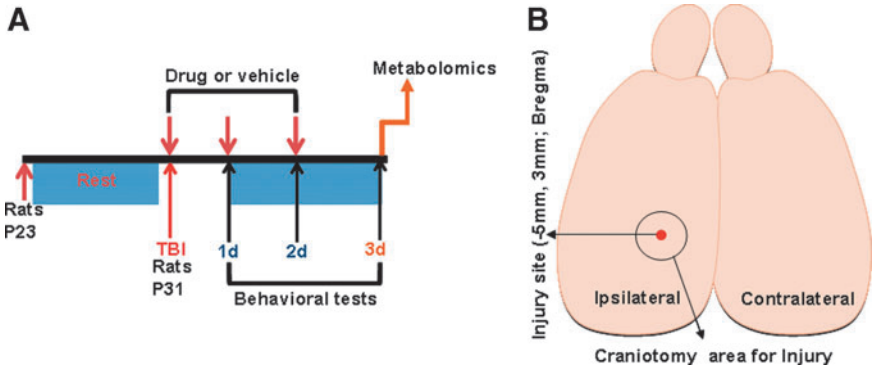

FIG. 1. (**A**) Schematic of the experimental design and time line assessing effects of drug or vehicle treatment on traumatic brain injury, behavioral and metabolomic assessments. (**B**) Schematic of the rat brain indicating the stereotaxic location of injury and craniotomy. Color image is available online.

using the standard microhomogenizer (Pro Scientific). A 500 μL of sample was taken out to a new Eppendorf tube and centrifuged at 4°C for 15 min at 14,000 rpm. Supernatants were collected and normalized to tissue weight.

The LC/MS measurements were performed on the brain extract samples using a Q ExactiveOrbitrap mass spectrometer (Thermo Scientific) coupled to a Vanquish UPLC system (Thermo Scientific). The Q Exactive operated in a polarity-switching mode. A Sequant ZIC-HILIC column; 2.1 × 150 mm i.d, (Merck. Co), was used for metabolite separation. Buffers consisted of high performance liquid chromatography (HPLC) buffer-A (100% acetonitrile), and HPLC buffer-B (pH = 9.0: 95% [vol/vol] water, 5% [vol/vol] acetonitrile, 20 mM ammonium hydroxide, 20 mM ammonium acetate). The HPLC flow rate was set at 150 μL/min, and gradients were from 85% to 30% for buffer A in 20 min followed by a wash with 30% buffer A and re-equilibration at 85% buffer A. Metabolites were identified based on exact mass within 5 ppm and standard retention times. Relative metabolite quantification was performed based on peak area for each identified metabolite.

Metabolite data analysis and statistics

Statistical comparisons between hemispheres of sham and TBI were made as shown in Figure 1B. Data analysis was performed using the software Metaboanalyst 3.0.[32,33] To minimize variations introduced during sample preparation effects of ion suppression, metabolite peak intensities were normalized to tissue wet-weight. Because of deviations from normality as tested by the Shapiro-Wilk test, data subsequently were log transformed and auto-scaled (mean-centered and divided by the standard deviation of each variable), effectively converting them to Z-scores. Plots of fold change in log scale were determined to efficiently represent metabolite concentration changes in both directions (increase or decrease).

Partial least squares discriminant analysis (PLS-DA) was used to determine the separation between groups of the metabolite variables through rotation of the principal components obtained by principal component analysis (PCA). This multivariate analysis was used because of the presence of more metabolite variables than observations in addition to correlation among the variables in the data.[34] The PLS-DA two-dimensional and three-dimensional score plots were generated from the first two and first three principal components, respectively, for classification. The PLS-DA analysis was also used for feature selection, and feature importance measures were generated (VIP: variable importance in projection). R^2X and R^2Y, the fraction of variation that the model explains in the independent variables (X) and dependent variables (Y) and Q^2Y: the predictive accuracy of the model was estimated by the PLS-DA cross-validation. These variables range between 0–1 with values >0.5 indicating good and >0.8 indicating outstanding predictive accuracies, respectively. Loading plots (top 25 variables) were used to determine the clustering of variables and whether their relationship within (weightings) scores changed in response to TBI.

To measure the impact of individual metabolite changes on biochemical pathways, metabolic pathway analysis (MetPA)[35] and metabolite set enrichment analysis (MSEA) [36] were performed. The MetPA combined results from pathway enrichment analysis with pathway topology analysis using a high-quality Kyoto Encyclopedia of Genes and Genomes metabolic pathway database. Data were analyzed using a pre-existing rat reference library with global test algorithm for MSEA and relative-between centrality algorithm for pathway topology analysis provided within the Metaboanalyst software.

Pathway enrichment analysis used metabolite concentration values to calculate *p* values based on the asymptotic distribution without using permutations. Because many pathways were tested simultaneously, *p* values were corrected for multiple comparisons using Holm-Bonferroni method (Holm *p*) and false discovery rate (FDR). Pathway topology analysis estimated node importance based on two node centrality measures—namely, degree centrality and betweenness centrality. While degree centrality represented the number of links converging on a node, betweenness centrality represented the number of shortest paths passing through the node. Different from the degree centrality measure focusing on local connectivity, the betweenness centrality measure focused on global network topology. Hence, our analysis used the betweenness centrality measure to calculate the pathway impact values in MetPA as implemented in our previous study.[16]

The MSEA directly investigates a set of functionally related metabolites without the need to pre-select metabolites based on some arbitrary cutoff threshold. Patterns of metabolites that are significantly enriched in biologically relevant pathways can be assessed.[36] It has the potential to identify subtle but consistent changes among a group of related compounds in a certain biological pathway. A quantitative enrichment analysis algorithm and a custom-made metabolite set library containing 36 metabolite sets based on metabolic pathways related to the detected brain metabolites, as implemented in our earlier studies,[16] was used as the reference library. The enrichment analyses considered the reference metabolome built based on our analytical platform of the current targeted brain metabolites. A global test algorithm using a generalized linear model was used to estimate a Q-statistic for each metabolite set describing the correlation between metabolite concentration profiles (X) and physiological outcomes (Y). The Q statistic for each metabolite was derived from the average of the Q statistics for each metabolite within the set. Statistical *p* values after MSEA were corrected for multiple comparisons using the Holm *p* and FDR.

Whisker stimulation-induced motor response (WSIMR)

To assess early sensorimotor defects, WSIMR was performed 24, 48, and 72 h after injury. The WSIMR test is an adaptation of a previously established whisker stimulation-induced paw placement test in adult animals.[37] We have modified this sensorimotor test successfully to developmental stage animals as established by our previous studies.[16,27] Animals were placed in a test cage and left to habituate for 1 min. Subsequently, whiskers on either side were stroked in a rostrocaudal direction using an applicator stick. Each trial consisted of multiple strokes at 3 Hz frequency, and up to 10 trials were performed on each side of the animal with an intertrial gap of 1 min.

Responses were scored on a scale of 0–5. Active avoidance by running away with 1–2 strokes = 5; with 1–2 strokes, quick head movement away from the stroking stick = 4; slower head movement after 1–2 strokes away from the stick = 3; head movement away from the stick after 3–6 strokes = 2; slower head movement after 3–6 strokes = 1, and no reaction to stroking beyond nine strokes = 0. An average score of the 10 trials was determined.

Forelimb usage test

The neural basis of spatial and motor behaviors, used as an assay of brain function, can be assessed by natural exploratory behavior in the rat. The forelimb usage test was a modified version of the cylinder test and provides a way to evaluate spontaneous forelimb usage in the home cage environment as demonstrated in our previous studies.[16] Each animal was observed for 5 min duration in a test cage 24, 48, and 72 h after injury. Active exploration of vertical surfaces by rearing up on the hind limbs and wall surface exploration with forelimbs were observed and scored. The number of independent wall placements observed for contralateral, ipsilateral, or both forelimbs were scored. Animals using both forelimbs simultaneously = 5; exploring cage wall with only the contralateral forelimb usage = 4; exploring cage wall with only ipsilateral forelimb usage = 3. Percentage forelimb usage within the 5 min observation duration was determined.

Results

The TBI was performed using the lateral FPI rat model on the left hemisphere (Fig. 1A) and randomly assigned to different treatment groups, with the first group not receiving any treatment, second TBI group receiving vehicle containing 10% dimethyl sulfoxide (DMSO) in saline, and the third TBI group receiving intraperitoneal kaempferol (1 mg/kg). Sensorimotor behavior was assessed using WSIMR and forelimb usage tests, respectively, during the acute/subacute stage at 24, 48, and 72 h after injury. After completion of behavioral monitoring, postmortem brains were removed at 72 h and extracted for metabolomics studies using LC/MS measurements.

Improved sensorimotor behaviors after kaempferol treatment

The TBI animal groups underwent sensorimotor behavioral assessments using the WSIMR and forelimb usage tests at 24, 48, and 72 h after TBI. Untreated and vehicle treated TBI animals showed no significant differences in WSIMR behavior. There was a significant interhemispheric asymmetry, with greater WSIMR deficit on contralateral whisker stimulation compared with ipsilateral (Fig. 2A,B). The WSIMR behavior in the current untreated and vehicle treated TBI animals was reproducible and comparable to that of our previous studies on this developmental TBI model.[27]

Kaempferol treated TBI animals showed significantly improved ipsilateral (Fig. 2A) and contralateral WSIMR scores (Fig. 2B) at all time points compared with vehicle. During forelimb usage assessments, TBI animals showed 34% usage of ipsilateral forelimb, 20% usage of contralateral forelimb, and 46% usage of both forelimbs simultaneously at all time points (Fig. 2C). Vehicle treated TBI animals also showed a similar trend of forelimb usage with no significant differences from the untreated TBI animals (Fig. 2C). Kaempferol treated animals, however, showed an increase in simultaneous usage of both forelimbs (70%). In addition, unlike the untreated and vehicle treated TBI animals, the interhemispheric

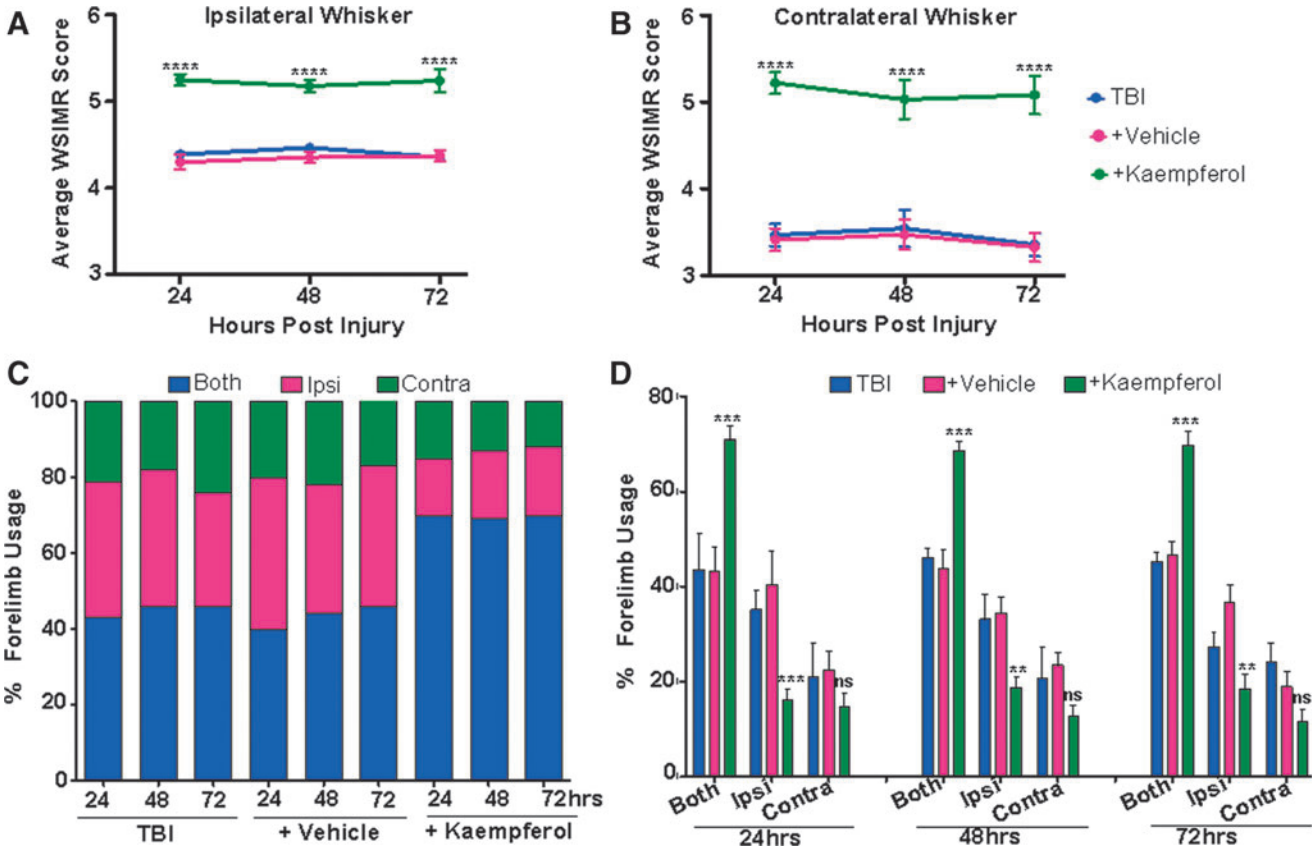

FIG. 2. Improved sensorimotor behaviors after kaempferol treatment. (**A**) Ipsilateral whisker stimulation: animals with traumatic brain injury (TBI) exhibited reduced whisker stimulation-induced motor response (WSIMR) in response (blue). Vehicle treated TBI animals (pink) did not differ from untreated TBI animals, whereas kaempferol significantly improved the WSIMR responses (green). (**B**) Contralateral whisker stimulation: TBI animals exhibited a relatively more intense reduction in WSIMR in response (blue). Vehicle treated TBI animals (pink) did not differ from untreated TBI animals, whereas kaempferol significantly improved the WSIMR responses (green). (**C**) Percentage forelimb usage in TBI, vehicle, and kaempferol treated animals. The TBI animals used both forelimbs simultaneously (blue) ~45% of the time, with an increased usage of only the ipsilateral forelimb (pink) (~34%) or only contralateral forelimb (green) (~20%), indicating profound motor functional deficits on both brain hemispheres after TBI. Vehicle treated animals exhibited forelimb defects, similar to untreated TBI animals. Kaempferol treatment improved both forelimb usage simultaneously to ~70% (blue), with reduced usage of only the ipsilateral (~18%) or only contralateral forelimb (~13%). (**D**) Percentage forelimb usage in untreated, vehicle, or kaempferol treated TBI animals. Kaempferol treated TBI animals showed improved usage of both forelimbs simultaneously. Significantly different; ***$p < 0.001$; **$p < 0.01$; two-way repeated measures analysis of variance. Data represent mean ± standard error of the mean. Color image is available online.

asymmetry in single forelimb usage was absent in kaempferol treated TBI animals (Fig. 2C, D).

Effect of no treatment or vehicle treatment on the TBI metabolome

Ipsilateral metabolome differences between sham versus untreated TBI animals were assessed and compared with sham versus vehicle treated TBI animals. Untreated TBI animals showed broad metabolic changes compared with sham with at least 25% metabolites showing greater than twofold change (Fig. 3A,B) and significant class separation by PLS-DA analysis (Fig. 3C–E). The MetPA analysis showed significant changes (Holm $p < 0.05$) related to glyoxylate and dicarboxylate metabolism, tricarboxylic acid (TCA) cycle, gycolysis and gluconeogenesis, vitamin B6 metabolism, pyruvate metabolism, and prominent amino acids (Fig. 4A). The MSEA also showed significant (Holm $p < 0.05$) fold enrichment in metabolite clusters related to oxidation of branched chain fatty acids, pyruvate metabolism, transfer of acetyl groups into mitochondria, glycolysis, and TCA cycle and several other metabolic pathways (Fig. 4B).

Similar to untreated TBI, vehicle treated TBI animals showed a broad metabolic shift compared with sham with at least 20% of the metabolites showing greater than twofold change (Fig. 5). The MetPA analysis showed significant changes (Holm $p < 0.05$) related to pyruvate metabolism, TCA cycle, nicotinate and nicotinamide metabolism, and glycolysis (Fig. 6A). Further, MSEA showed significant (Holm $p < 0.05$) fold enrichment in several critical metabolite clusters related to various amino acid metabolic pathways, pyruvate metabolism, glycolysis and gluconeogenesis, TCA cycle, glucose-alanine cycle, mitochondrial beta-oxidation of short fatty acids, fatty acid metabolism, betaine metabolism, and bile acid biosynthesis (Fig. 6B).

To obtain accurate effects of vehicle treatment, we compared the ipsilateral untreated and vehicle treated TBI metabolomes. As shown in Figure 7, greater than twofold changes were observed in a small group of metabolites (3.6% of the targeted metabolites). Adenosine diphosphate (ADP) levels decreased, whereas 2-

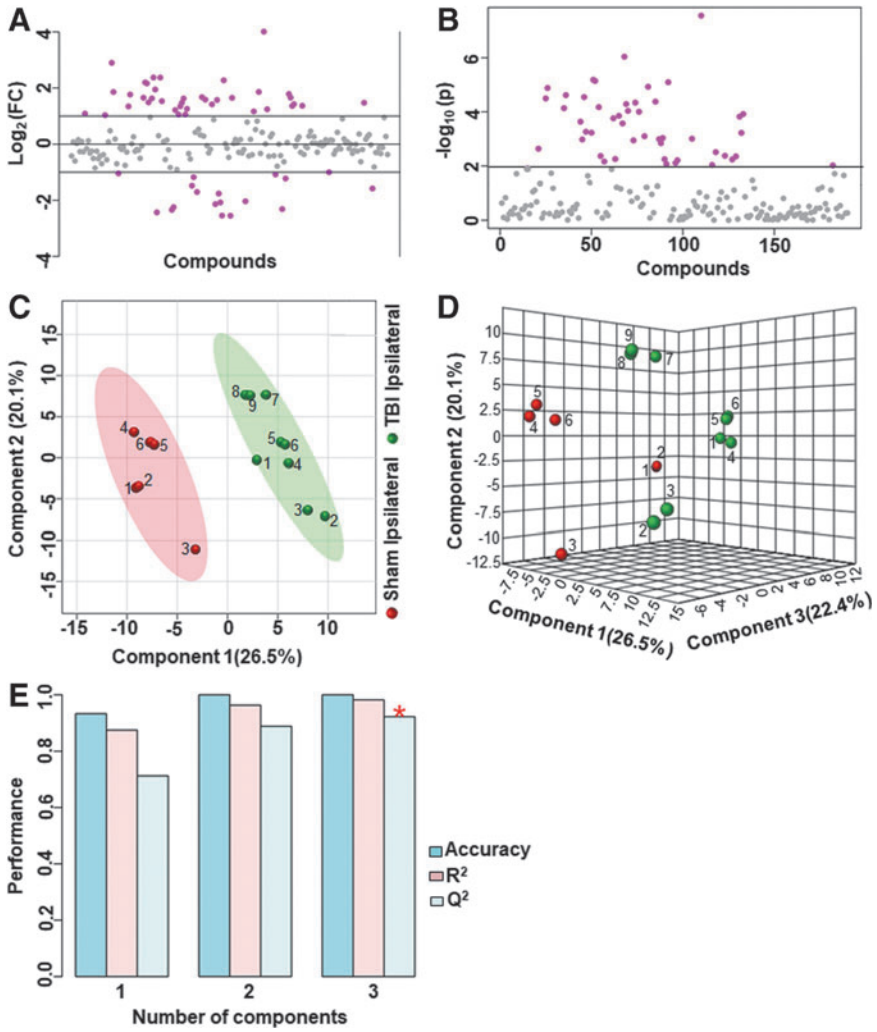

FIG. 3. Ipsilateral metabolic differences between sham and untreated animals with traumatic brain injury (TBI) (**A**) Ipsilaterally, 25% of the metabolites showed a twofold change between sham animals and untreated TBI animals. (**B**) There were 22% of the targeted metabolites that were significantly different ($p < 0.01$). (**C**) Partial least squares discriminant analysis PLS-DA two-dimensional scores plot (**D**) PLS-DA three-dimensional scores plot showed a good class separation. (**E**) Cross validation values of the PLS-DA model. Accuracy: 1.0, R^2: 0.98, Q^2: 0.92, suggested a very high accuracy of the model. Color image is available online.

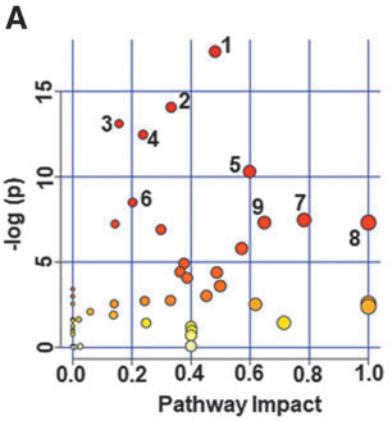

No	Metabolic pathway/Metabolism	P value	Holm P	FDR	Impact
1	Glyoxylate and dicarboxylate	0.00000003	0.000001	0.000001	0.48
2	Citrate cycle (TCA cycle)	0.0000007	0.00003	0.00001	0.33
3	Vitamin B6	0.000002	0.00009	0.00003	0.15
4	Glycolysis or Gluconeogenesis	0.000003	0.0001	0.00004	0.23
5	Glycine, serine and threonine	0.00003	0.001	0.0003	0.59
6	Pyruvate metabolism	0.0002	0.009	0.001	0.20
7	Alanine, aspartate, & Glutamate	0.0005	0.02	0.003	0.78
8	Phenylalanine, tyrosine & tryptophan biosynthesis	0.0006	0.02	0.003	1.0
9	Phenylalanine	0.0006	0.02	0.003	0.64

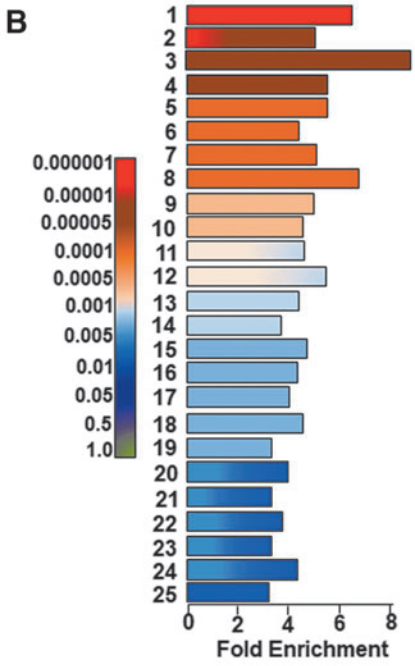

No	Metabolite set	P value	Holm P	FDR
1	Oxidation of branched chain fatty acids	0.0000002	0.000006	0.000006
2	Pyruvate metabolism	0.000001	0.00003	0.00001
3	Vitamin B6 metabolism	0.000002	0.00006	0.00001
4	Transfer of acetyl groups into mitochondria	0.000002	0.00006	0.00001
5	Glycolysis	0.000003	0.0001	0.00002
6	Histidine metabolism	0.000004	0.0001	0.00002
7	Citric acid cycle	0.000007	0.0002	0.00003
8	Phenylalanine and tyrosine metabolism	0.000008	0.0002	0.00003
9	Betaine metabolism	0.00002	0.0006	0.00008
10	Glutamate metabolism	0.00002	0.0006	0.00009
11	Gluconeogenesis	0.00008	0.001	0.0002
12	Thiamine metabolism	0.00008	0.001	0.0002
13	Pentose phosphate pathway	0.0002	0.004	0.0005
14	Urea cycle	0.0002	0.005	0.0006
15	Nicotinate and nicotinamide metabolism	0.0003	0.007	0.0008
16	Glycine and serine metabolism	0.0003	0.007	0.0008
17	Tyrosine metabolism	0.0004	0.008	0.0009
18	Phosphatidylcholine biosynthesis	0.0006	0.009	0.001
19	Aspartate metabolism	0.0006	0.009	0.001
20	Ammonia recycling	0.001	0.02	0.002
21	Arginine and proline metabolism	0.001	0.02	0.002
22	Tryptophan metabolism	0.002	0.02	0.003
23	Methionine metabolism	0.003	0.03	0.004
24	Malate-aspartate shuttle	0.003	0.03	0.005
25	Phospholipid biosynthesis	0.006	0.05	0.008

FIG. 4. Ipsilateral pathway impact analysis between sham and untreated animals with traumatic brain injury (TBI). (**A**) Metabolic pathway analysis (MetPA): Left panel-node colors are based on *p* values and node size on pathway impact values. Table on the right shows significantly affected metabolic pathways. (**B**) Metabolite set enrichment analysis (MSEA): Left panel y-axis indicates the metabolite sets based on the Holm *p* values and x-axis indicates the fold enrichment. Table on the right shows affected pathways relevant to significantly enriched metabolite sets where broad metabolomic shift affecting several pathways can be observed in the untreated TBI group compared with sham. FDR, false discovery rate. Color image is available online.

isopropyl-3-oxosuccinate, kynurenic acid, L-dihydroorotic acid, NAA, phosphoenolpyruvate, and spermidine levels increased (Fig. 7A,B). Multivariate analyses using PLS-DA (Fig. 7C,D) showed a partial class separation along with a low accuracy of the PLS-DA model (accuracy = 0.68, R^2 value = 0.84, Q^2 value = 0.11). The MetPA and MSEA showed no significant changes in any of the metabolic pathways (Fig. 7E,F; all Holm *p* values being >0.05). Comparing contralateral hemispheres between the untreated and vehicle treated TBI animals, greater than twofold changes occurred in only about 2% of the targeted metabolites. Citric acid, hippuric acid, phosphoenolpyruvate and spermidine levels increased in the vehicle treated TBI versus untreated TBI (Fig. 8A,B).

Multivariate analyses using PLS-DA showed a partial class separation (Fig. 8C,D), along with a low accuracy value of the PLS-

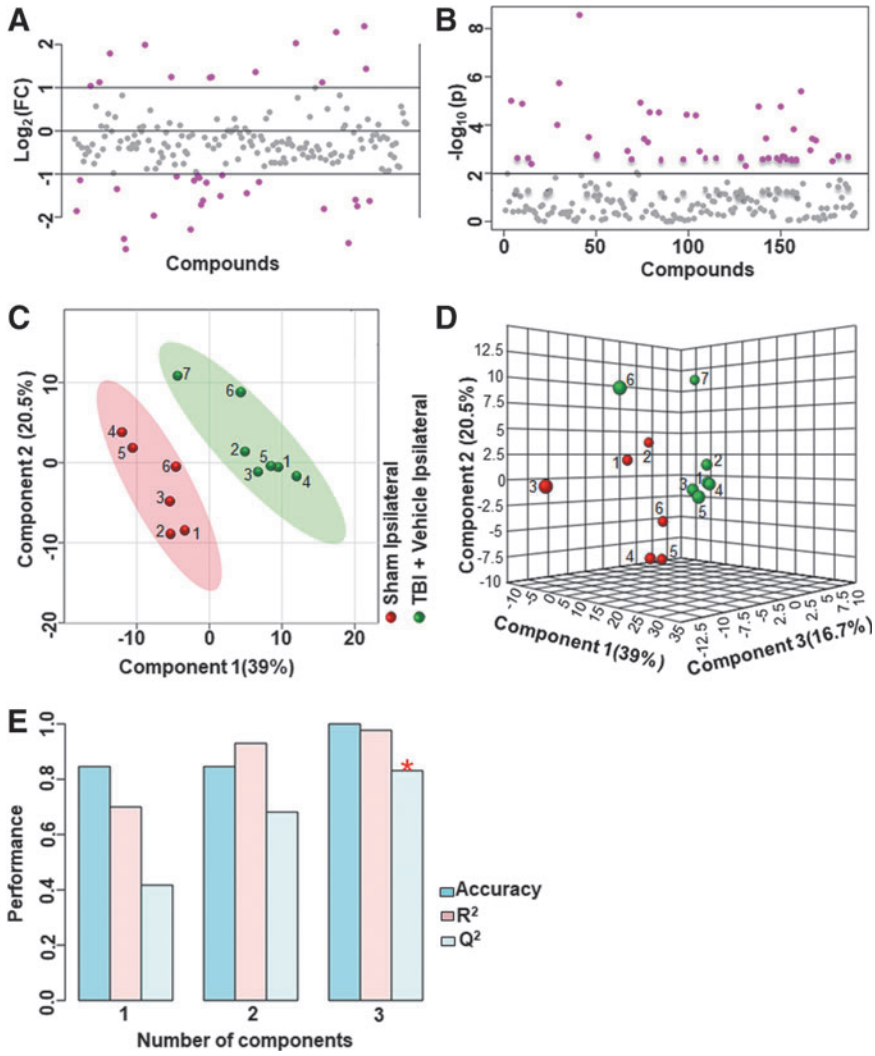

FIG. 5. Ipsilateral metabolic differences between sham and vehicle treated animals with traumatic brain injury (TBI). (**A**) Ipsilaterally, 20% of the metabolites showed a two-fold change between sham animals and vehicle treated TBI animals. (**B**) There were 15% of the targeted metabolites that were significantly different. (**C**) Partial least squares discriminant analysis (PLS-DA) two-dimensional scores plot (**D**) PLS-DA three-dimensional scores plot showed a good class separation. (**E**) Cross validation values of the PLS-DA model. Accuracy: 0.79, R^2: 0.90, Q^2: 0.91, suggested a very high accuracy of the model. Color image is available online.

DA model (accuracy = 0.75, R^2 value = 0.87, Q^2 value = 0.18). The MetPA and MSEA analyses also showed no significant change in any metabolic pathways (Fig. 8E,F, all Holm p values being >0.05). These results highlight an insignificant impact of vehicle treatment on any metabolic pathway after TBI.

Kaempferol effects on the TBI metabolome

Assessing the impact of kaempferol treatment on the TBI metabolome, metabolic differences between vehicle and kaempferol treated animal groups were performed. On the ipsilateral hemisphere, vehicle and kaempferol treated TBI animals showed greater than twofold changes in about 7% of the targeted metabolites (Fig. 9A). Citric acid, L-acetylcarnitine, hexanoylcarnitine, and propionylcarnitine levels decreased after kaempferol treatment, whereas R-lipoic acid, acetylphosphate, ADP, gluconic acid, glucosamine 6-phosphate, fructose 6-phophate, NAA, nicotinamide dinucleotide (NAD), oxoglutaric acid, and uric acid levels increased (Fig. 9B). Multivariate PLS-DA analysis (Fig. 9C, D) showed distinct class separation with a high accuracy of the PLS-DA model (accuracy = 1.0, R^2 value = 0.95, Q^2 value = 0.78). The MetPA showed significant changes (Holm $p < 0.05$) in pathways related to the TCA cycle, alanine, aspartate, and glutamate metabolism, D-glutamine/D-glutamate metabolism, and pyruvate metabolism (Fig. 10A). The MSEA analysis also showed significant (Holm $P < 0.05$) fold enrichment in several critical metabolite clusters related to transfer of acetyl groups into mitochondria, glucose-alanine cycle, TCA cycle, glycolysis, malate-aspartate shuttle, oxidation of branched chain fatty acids, and urea cycle (Fig. 10B).

On the contralateral hemisphere, kaempferol treated TBI animal groups showed greater than twofold changes in only three metabolites (1.5% of the total targeted metabolites) compared with vehicle (Fig. 11A). The NAD, α-ketoglutarate (α-KG), and ureidosuccinate levels increased with kaempferol treatment compared with vehicle treated TBI animals (Fig. 11B). Multivariate analyses using PLS-DA (Fig. 11C,D), showed no class separation with low model accuracy (accuracy = 0.64, R^2 value = 0.92, Q^2 value = −0.02). Further, no significant impact of kaempferol was

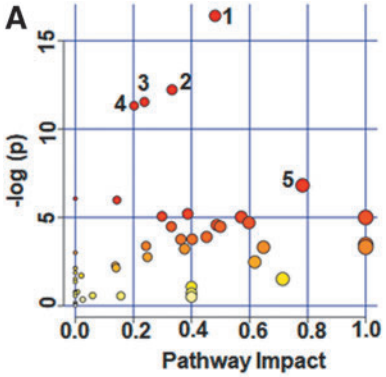

No	Metabolic pathway/Metabolism	P value	Holm P	FDR	Impact
1	Glyoxylate and dicarboxylate	0.00000007	0.000003	0.000003	0.48
2	Citrate cycle (TCA cycle)	0.000004	0.0002	0.0001	0.33
3	Glycolysis or Gluconeogenesis	0.000009	0.0004	0.0001	0.23
4	Pyruvate metabolism	0.00001	0.0005	0.0001	0.20
5	Alanine, aspartate and glutamate	0.001	0.04	0.01	0.78

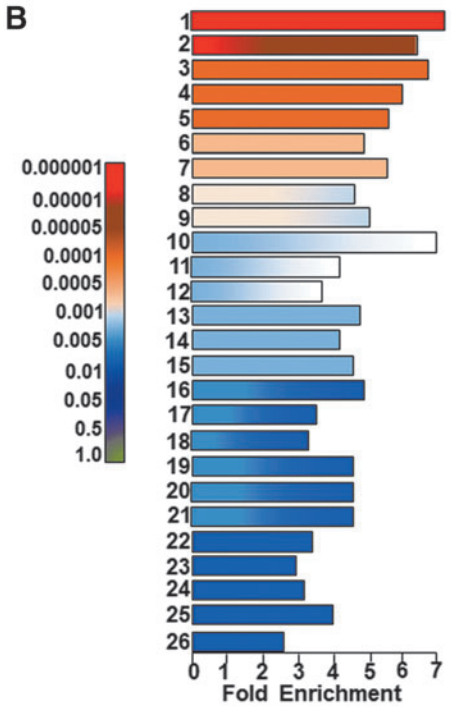

No	Metabolite set	P value	Holm P	FDR
1	Oxidation of branched chain fatty acids	0.0000004	0.000001	0.000001
2	Glycolysis	0.0000009	0.00002	0.00001
3	Pyruvate metabolism	0.000007	0.0002	0.00007
4	Transfer of acetyl groups into mitochondria	0.00001	0.0003	0.00007
5	Citric acid cycle	0.00001	0.0003	0.00007
6	Histidine metabolism	0.00002	0.0007	0.0001
7	Gluconeogenesis	0.00002	0.0007	0.0001
8	Urea cycle	0.00004	0.001	0.0001
9	Glutamate metabolism	0.00005	0.001	0.0001
10	Thiamine metabolism	0.00005	0.002	0.0001
11	Ammonia recycling	0.00009	0.002	0.0002
12	Glycine and serine metabolism	0.0001	0.002	0.0003
13	Malate-aspartate shuttle	0.0002	0.005	0.0006
14	Tyrosine metabolism	0.0003	0.007	0.0008
15	Glucose alanine cycle	0.0004	0.008	0.0009
16	Nicotinate and nicotinamide metabolism	0.0008	0.01	0.001
17	Aspartate metabolism	0.001	0.01	0.002
18	Phenylalanine and tyrosine metabolism	0.001	0.02	0.002
19	Pentose phosphate pathway	0.001	0.02	0.003
20	Phosphatidylcholine biosynthesis	0.002	0.03	0.004
21	Aminosugar metabolism	0.002	0.03	0.004
22	Tryptophan metabolism	0.003	0.04	0.005
23	Methionine metabolism	0.004	0.04	0.005
24	Arginine and proline metabolism	0.004	0.04	0.005
25	Glutathione metabolism	0.006	0.05	0.007
26	Purine metabolism	0.007	0.05	0.009

FIG. 6. Ipsilateral pathway impact analysis between sham and vehicle treated animals with traumatic brain injury (TBI). (**A**) Metabolic pathway analysis (MetPA): Left panel-node colors are based on *p* values and node size on pathway impact values. Table on the right shows significantly affected metabolic pathways. (**B**) Metabolite set enrichment analysis (MSEA): Left panel y-axis indicates the metabolite sets based on the Holm *p* values and x-axis indicates the fold enrichment. Table on the right shows affected pathways relevant to significantly enriched metabolite sets, where broad metabolomic shift affecting several pathways can be observed in the TBI+ vehicle treated group. FDR, false discovery rate. Color image is available online.

observed on any metabolic pathway in the contralateral hemisphere as assessed by the MetPA and MSEA analyses (Fig. 11E,F; all Holm *p* values being >0.05).

Discussion

The lateral FPI is highly diffusive affecting the acute/subacute (72 h post-TBI) metabolite components with a relatively higher intensity in the ipsilateral (injury lateralized hemisphere) compared with contralateral (Fig. 1B).[16] The broad post-TBI metabolomic disturbance with more ipsilateral intensity does not translate to significant ipsilateral brain lesions assessed by conventional T2-weighted magnetic resonance imaging (MRI), two months after TBI.[38] Diffusion tensor imaging (DTI) based morphological characterization, however, could detect long-term microstructural abnormalities, and functional MRI (fMRI) could detect functional abnormalities related to neural connectivity and cerebrovascular reactivity with a relatively more intense ipsilateral impact.[38]

Stimulation-induced neural circuit activity as assessed by functional laser Doppler imaging (fLDI) of whisker deflection-

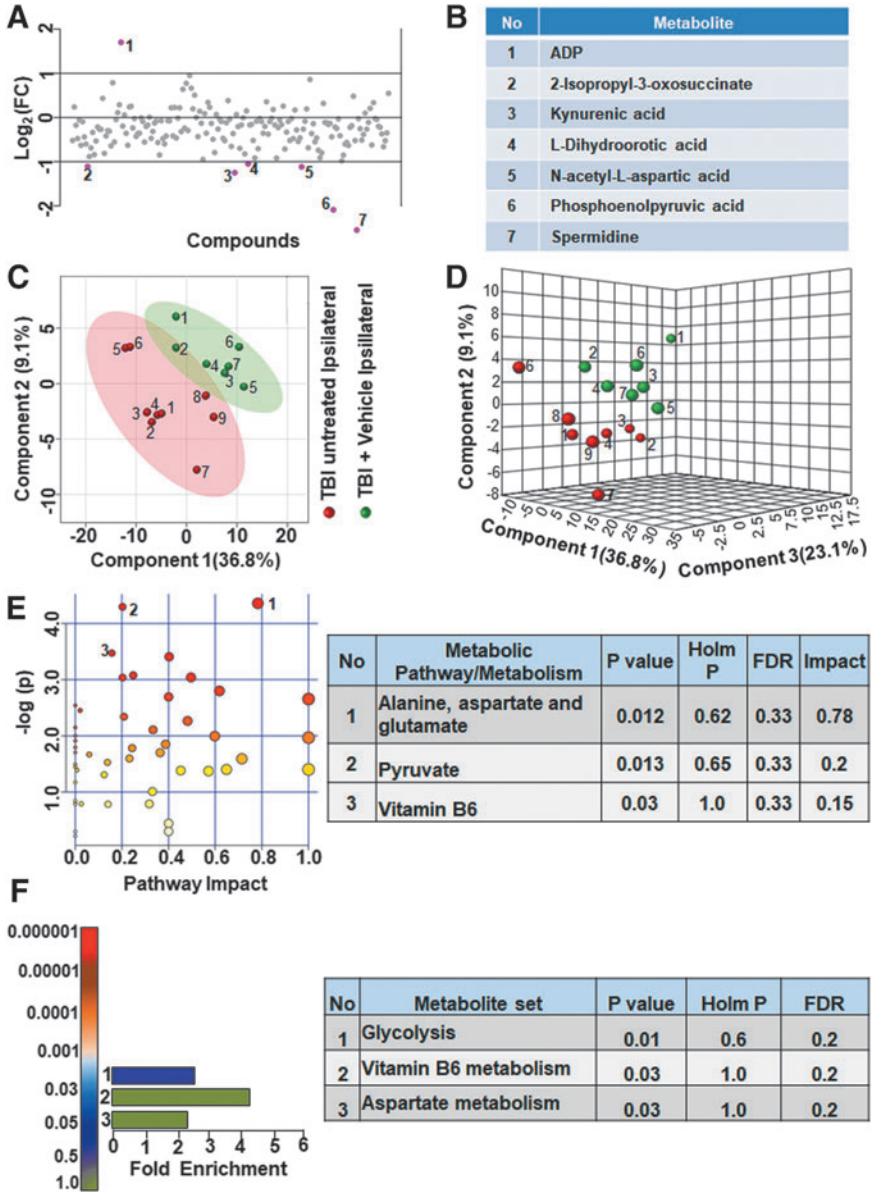

No	Metabolite
1	ADP
2	2-Isopropyl-3-oxosuccinate
3	Kynurenic acid
4	L-Dihydroorotic acid
5	N-acetyl-L-aspartic acid
6	Phosphoenolpyruvic acid
7	Spermidine

No	Metabolic Pathway/Metabolism	P value	Holm P	FDR	Impact
1	Alanine, aspartate and glutamate	0.012	0.62	0.33	0.78
2	Pyruvate	0.013	0.65	0.33	0.2
3	Vitamin B6	0.03	1.0	0.33	0.15

No	Metabolite set	P value	Holm P	FDR
1	Glycolysis	0.01	0.6	0.2
2	Vitamin B6 metabolism	0.03	1.0	0.2
3	Aspartate metabolism	0.03	1.0	0.2

FIG. 7. Ipsilateral metabolic differences between untreated and vehicle treated animals with traumatic brain injury **(TBI).** (**A, B**) There were 4% of the metabolites that showed a twofold change in the ipsilateral hemisphere between untreated and vehicle treated TBI animals. (**C**) Partial least squares discriminant analysis (PLS-DA) two-dimensional scores plot, (**D**) PLS-DA three-dimensional scores plot showed partial class separation between untreated (red dots) versus vehicle treated TBI (green dots) in the ipsilateral hemisphere. (**E**) Metabolic pathway analysis (MetPA): Left panel-node colors are based on *p* values and node size on pathway impact values. Table on the right shows affected metabolic pathways. None of the pathways were significantly affected between untreated and vehicle treated TBI animals. (**F**) Metabolite set enrichment analysis (MSEA): Left panel of **E** and **F** y-axis indicates metabolite sets based on the Holm *p* value and x-axis indicates the fold enrichment. Table on the right panel indicates affected pathways relevant to significantly enriched metabolite sets. None of the pathways were found to be significantly affected between untreated and vehicle treated TBI animals. FDR, false discovery rate. Color image is available online.

induced somatosensory ($S1_{BF}$) cerebral blood flow responses indicated substantially changed ipsilateral circuit activity compared with contralateral two months after TBI. [27] The current fluid percussion induced lateralized TBI model with differential brain hemispheric metabolomic perturbation and neurodegeneration at the acute/subacute stage[16] translated to proportional morphological and functional changes at two months after TBI.[27,38] Hence, interhemispheric metabolomic comparisons of TBI outcome after kaempferol treatment enabled the assessment of the potential early mechanisms leading to the observed long term (2 months post-TBI) improvement in ipsilateral brain functional activity and behavior. [27]

As observed by the current results (Fig. 3–6 and Supplementary Table S1), untreated and vehicle treated TBI metabolomes showed comparable metabolic shifts from sham in the ipsilateral hemisphere. This was corroborated by further ipsilateral comparison between untreated and vehicle treated TBI groups, which showed no significant differences in PLS-DA (Fig. 7C, D), MetPA, and MSEA analyses (Fig. 7E, F).

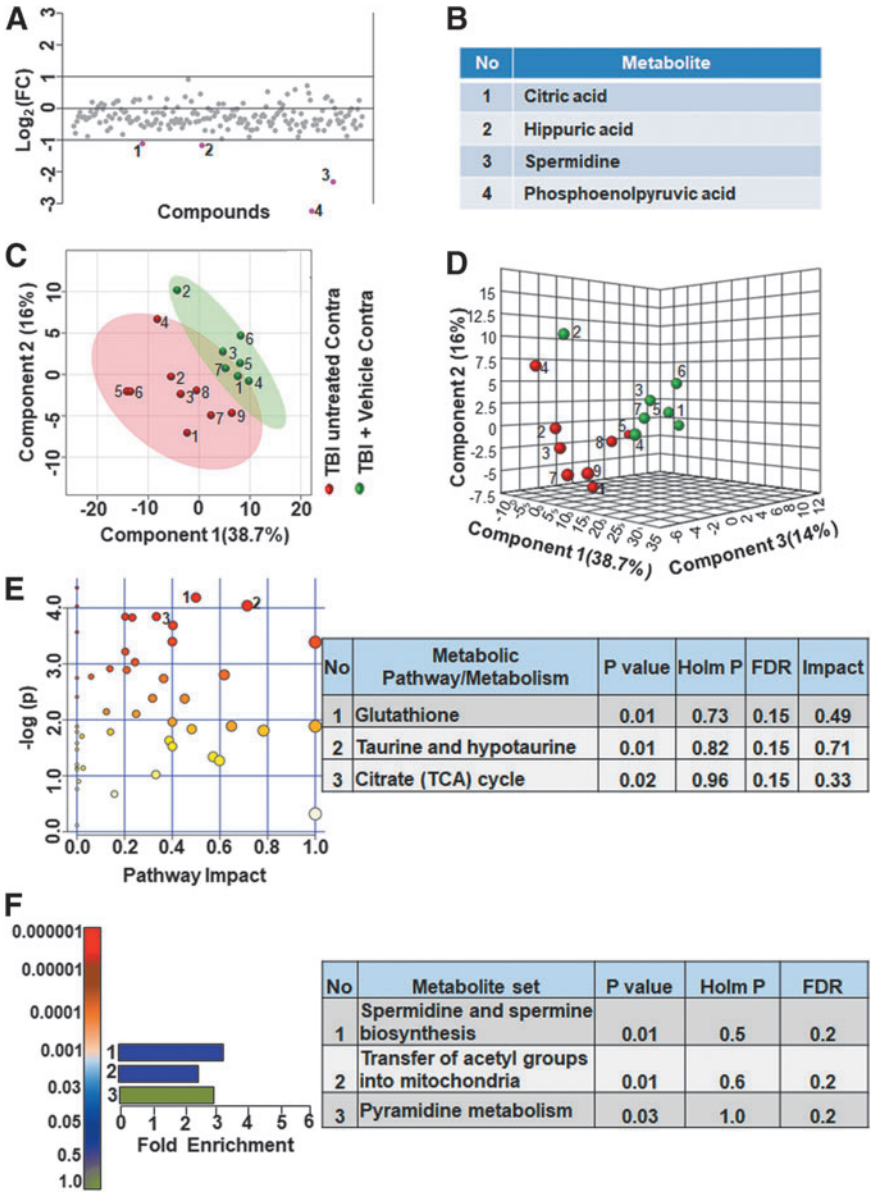

FIG. 8. Contralateral metabolic differences between untreated and vehicle treated animals with traumatic brain injury. (**A, B**) Two percent of the metabolites showed a twofold change in the contralateral hemisphere between untreated and vehicle treated TBI animals. (**C**) Partial least squares discriminant analysis (PLS-DA) two-dimensional scores plot, (**D**) PLS-DA three-dimensional scores plot showed partial class separation between untreated (red dots) versus vehicle treated TBI (green dots) in the contralateral hemisphere. (**E**) Metabolic pathway analysis (MetPA): Left panel-node colors are based on *p* values and node size on pathway impact values. Table on the right shows affected metabolic pathways. None of the pathways were significantly affected between untreated and vehicle treated TBI animals. (**F**) Metabolite set enrichment analysis (MSEA): Left panel y-axis indicates metabolite sets based on the Holm *p* value and x-axis indicates the fold enrichment. Table on the right panel of **E** and **F** indicates affected pathways relevant to significantly enriched metabolite sets. None of the pathways were found to be significantly affected between untreated and vehicle treated animals. FDR, false discovery rate. Color image is available online.

The DMSO vehicle treatment has been shown to provide a protective effect by reducing neuronal loss in rodent cerebral ischemia models.[39] Although an increase in NAA and spermidine were observed, indicating a possible neuroprotective effect of the current 10% DMSO in saline vehicle (Fig. 7B), the absence of any pathway-specific metabolic changes in vehicle treated TBI animals or behavioral differences (Fig. 2A–D) indicated no significant vehicle-dependent effects on the TBI metabolome or behavioral outcome.

Kaempferol treatment showed specific effects on several mitochondrial oxidative metabolism substrates and products. In vehicle treated TBI animals versus sham animals, levels of pyruvate, α-KG, oxaloacetate, and co-factor NAD^+ decreased along with increased citrate levels, signifying a decrease in TCA cycle flux (Supplementary Table S1). Kaempferol treatment, however, reversed the decline in TBI-induced TCA cycle flux with a relatively more intense ipsilateral impact compared with contralateral (Fig. 9, 10, 11). Although ipsilateral pyruvate levels did not improve after kaempferol treatment, levels of acetyl phosphate, a metabolite of pyruvate, increased (Fig. 9B). Acetyl phosphate produces acetyl CoA, acetate, and adenosine triphosphate, all important components and

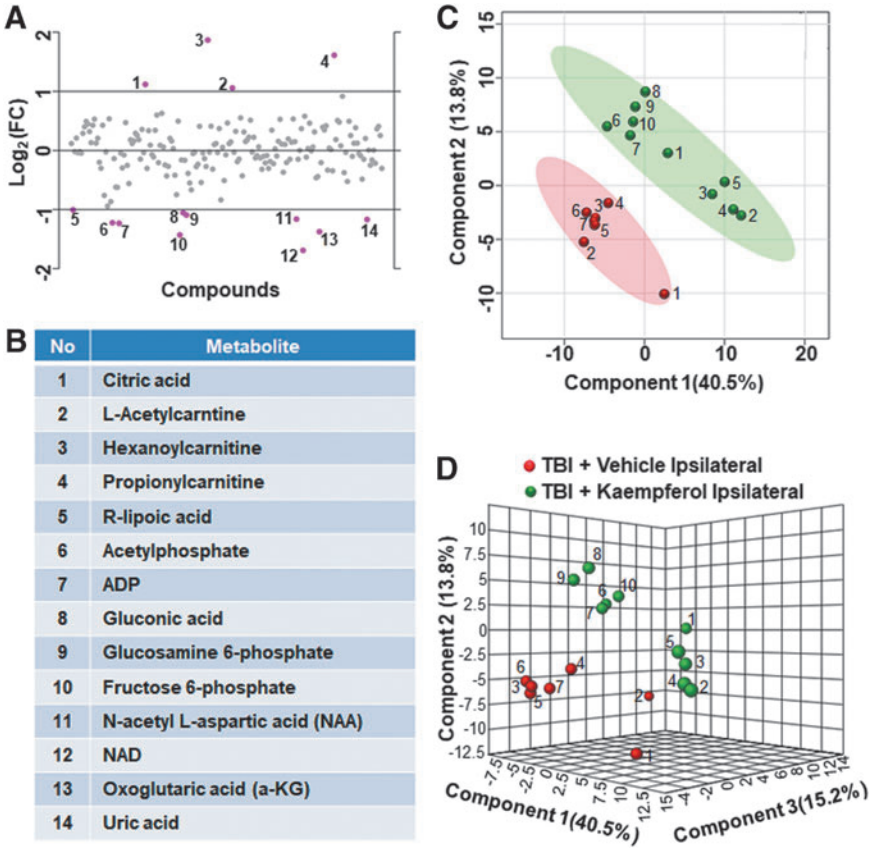

B

No	Metabolite
1	Citric acid
2	L-Acetylcarntine
3	Hexanoylcarnitine
4	Propionylcarnitine
5	R-lipoic acid
6	Acetylphosphate
7	ADP
8	Gluconic acid
9	Glucosamine 6-phosphate
10	Fructose 6-phosphate
11	N-acetyl L-aspartic acid (NAA)
12	NAD
13	Oxoglutaric acid (a-KG)
14	Uric acid

FIG. 9. Kaempferol treatment on traumatic brain injury (TBI) metabolome in the ipsilateral hemisphere. (**A, B**) Ipsilaterally, about 7% of the metabolites showed a two-fold change between vehicle treated and kaempferol treated TBI animals. (**C**) Partial least squares discriminant analysis (PLS-DA) two-dimensional scores plot, (**D**) PLS-DA three-dimensional scores plot showed distinct ipsilateral class separation between vehicle treated (red dots) versus kaempferol treated TBI animals (green dots). Color image is available online.

products of mitochondrial oxidative metabolism. A highly specific mitochondrial site of action of kaempferol could be inferred by the selective mitochondrial metabolite changes across both ipsilateral (Fig. 9) and contralateral hemispheres (Fig. 11).

A TBI leads to a broad spectrum of pathological consequences ranging from blood–brain barrier, cerebrovascular dysfunction,[40] loss of mitochondrial populations followed by excitotoxic neural death,[18,41] microglial proliferation, Ca^{2+} deregulation and protein degradation mediated delayed axonal damage,[42] proinflammatory cytokines,[43] and post-synaptic modification of neural circuits.[18,41,42,44] Each of these detrimental outcomes, although temporally asynchronous after injury,[45] may have early molecular origins potentially reflected by changes in relevant metabolic pathways. Hence, preservation of energy metabolism can have upstream beneficial consequences on several energy requiring pathways, some of them crucial for cellular repair after TBI.

Recently, we have characterized the relative intensities of different metabolic pathways perturbed because of a developmental TBI and found energy metabolism (TCA cycle and glycolysis) the most affected followed by one-carbon/folate, neurotransmitters/neuromodulator, amino acid and fatty acid metabolism (data not shown). As the TBI pathology is wide ranging,[44] presenting with numerous therapeutic targets, energy metabolic protection as a treatment strategy may have the highest impact in improving TBI outcomes because of its stabilizing effect on multiple downstream pathways.

Amino acid and fatty acid metabolism were significantly impacted by developmental TBI, although relatively lesser in impact compared with energy metabolism. This indicated continued inability of the injured brain to mobilize lipid constituents for membrane synthesis related to neural/synaptic integrity or repair. An important observation in both untreated and vehicle treated TBI animals was the increased levels of acyl carnitines, indicating reduced mitochondrial TCA cycle flux relative to fatty acid, glucose, and/or amino acid oxidation. The carnitine shuttle is essential to prevent accumulation of long chain fatty acids and long chain acyl-CoAs, which are deleterious to neural survival.[46] In the developing brain, the acetyl moiety is oxidized for energy and incorporated into neurotransmitters and lipids.[47] Mitochondria are particularly vulnerable to high concentrations of acyl carnitines[48] and L-carnitine supplementation, which restores the carnitine shuttle homeostasis, has been found to be protective in many neurodegenerative pathologies,[46] including pediatric models of TBI.[49]

The ability of kaempferol to decrease acyl carnitines compared with vehicle and maintaining their concentrations, similar to sham levels, indicated the ability of kaempferol to preserve the post-TBI carnitine shuttle homeostasis. This could lead to beneficial consequences of improved mitochondrial and cellular membrane integrity. Decreased acyl carnitines can also ameliorate oxidative stress, and we assessed whether significant antioxidative effects of kaempferol were present at the current 1 mg/kg dose treatments by observing the ratio of reduced and oxidized forms of glutathione

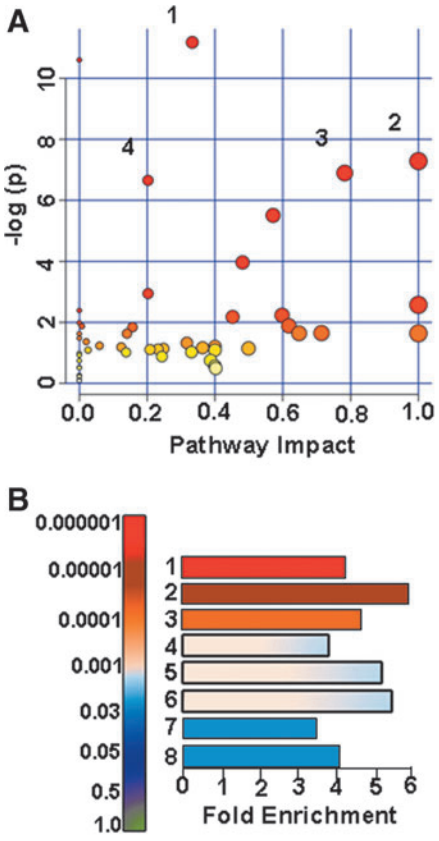

No.	Metabolic Pathway/Metabolism	P value	Holm P	FDR	Impact
1	Citric acid cycle	0.00001	0.0006	0.0006	0.33
2	D-glutamine and D-glutamate	0.0006	0.03	0.008	1.0
3	Alanine, aspartate and glutamate	0.001	0.04	0.01	0.78
4	Pyruvate metabolism	0.001	0.05	0.01	0.20

No.	Metabolite set	P value	Holm P	FDR
1	Transfer of acetyl groups into mitochondria	0.00000003	0.000001	0.000001
2	Glucose-alanine cycle	0.0000009	0.00003	0.00001
3	Citric acid cycle	0.00001	0.0004	0.0001
4	Tyrosine metabolism	0.00003	0.001	0.0002
5	Malate-aspartate shuttle	0.00006	0.002	0.0004
6	Oxidation of branched chain fatty acids	0.0001	0.003	0.0007
7	Urea cycle	0.001	0.03	0.005
8	Glycolysis	0.001	0.03	0.005

FIG. 10. Kaempferol treatment improved ipsilateral oxidative metabolism in TBI animals with traumatic brain injury (TBI). (**A**) Metabolic pathway analysis (MetPA): Left panel-node colors are based on *p* values and node size on pathway impact values. Table on the right shows significantly affected metabolic pathways. (**B**) Metabolite set enrichment analysis (MSEA): Left panel y-axis indicates the metabolite sets based on the Holm *p* values and x-axis indicates the fold enrichment. Table on the right shows affected pathways relevant to significantly enriched metabolite sets. The tricarboxylic acid cycle metabolites seem to be prominently affected by kaempferol treatment. FDR, false discovery rate. Color image is available online.

(GSH/GSSG) from the metabolite readouts (Metabolite No.74 and 151, respectively; Supplementary Table S1). Although GSH decreased significantly in untreated and vehicle treated TBI when compared with sham, no significant differences were observed in the GSH/GSSG ratio in vehicle versus kaempferol treated TBI conditions. An insignificant antioxidant effect of kaempferol at the current dose of 1 mg/kg was expected because antioxidative effects of kaempferol become significant only at relatively larger dose ranges as discussed in our previous study.[27]

Maintained mitochondrial ion homeostasis by facilitating mitochondrial Ca^{2+} uptake and cycling through kaempferol-induced enhancement of the mCU channel activity[50,51] seemed to preserve mitochondrial integrity/function and oxidative metabolism after a developmental TBI. The improved energy metabolic state after TBI, advantageous to several secondary cellular repair processes, resulted in improved neural viability and behavioral outcomes (Fig. 2). Because the behavioral experiments were unblinded, potential observer bias was a limitation. The effect sizes of the behavioral differences, however, were sufficiently large that this confound may not significantly affect the conclusions.

Conclusions

The acute/subacute stage metabolome of untreated, vehicle, and kaempferol treated TBI groups indicated a predominantly mitochondrial mechanism of action of kaempferol. While the primary effect of kaempferol was on mitochondrial oxidative metabolism indicated by high impact in the MetPA and MSEA analyses, other

FIG. 11. Kaempferol treatment on traumatic brain injury (TBI) metabolome in the contralateral hemisphere. (**A, B**) Contralaterally, about 1.5% of the metabolites showed a twofold difference between vehicle and kaempferol treated TBI animals. (**C**) Partial least squares discriminant analysis (PLS-DA) two-dimensional scores plot, (**D**) PLS-DA three-dimensional scores plot showed partial class separation between vehicle treated (red dots) versuss kaempferol treated TBI animals (green dots) in the contralateral hemisphere. (**E**) Metabolic pathway analysis (MetPA): Left panel-node colors are based on *p* values and node size on pathway impact values. Table on the right shows significantly affected metabolic pathways. None of the pathways were significantly affected. (**F**) Metabolite set enrichment analysis (MSEA): Left panel y-axis indicates the metabolite sets based on the Holm *p* values and x-axis indicates the fold enrichment. Table on the right shows affected pathways relevant to significantly enriched metabolite sets. None of the pathways were significantly affected. FDR, false discovery rate. Color image is available online.

A

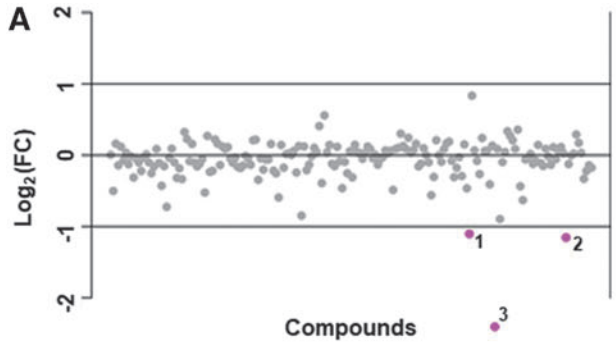

B

No	Metabolite
1	NAD
2	Ureidosuccinic acid
3	Oxoglutaric acid

C

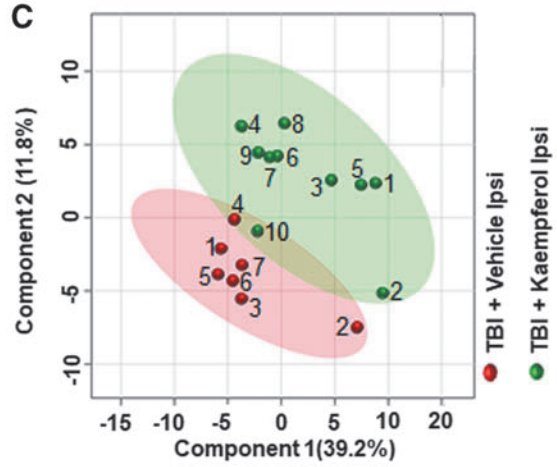

D

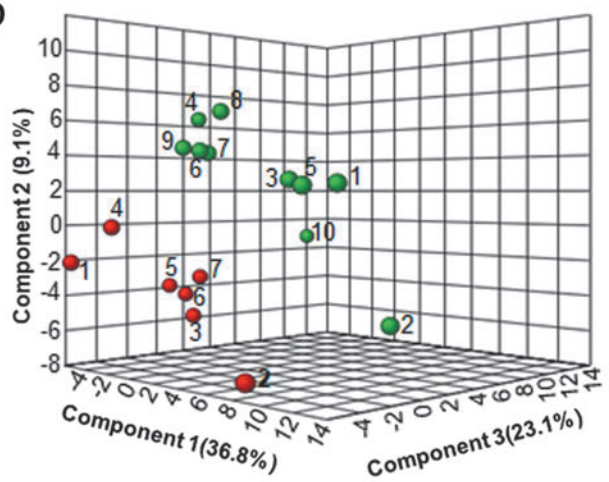

E

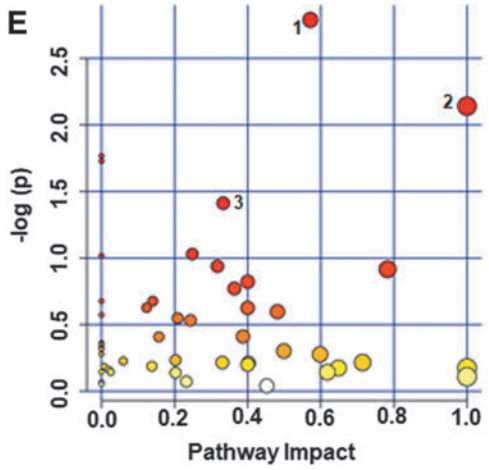

No	Metabolic Pathway/Metabolism	P value	Holm P	FDR	Impact
1	Nicotinate and nicotinamide	0.06	1.0	0.9	0.57
2	D-glutamine and glutamate	0.1	1.0	0.9	1.0
3	Citrate (TCA) cycle	0.2	1.0	0.9	0.33

F

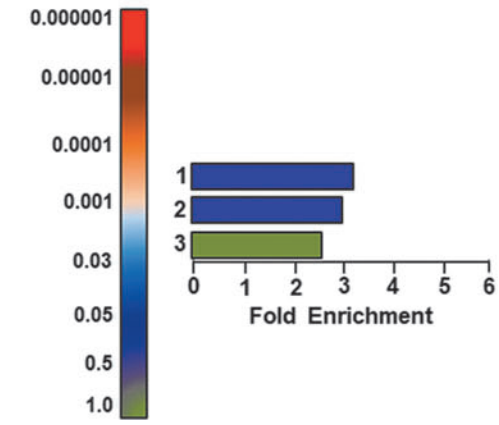

No	Metabolite set	P value	Holm P	FDR
1	Glucose-alanine cycle	0.005	0.1	0.1
2	Malate-aspartate shuttle	0.01	0.4	0.2
3	Cardiolipin biosynthesis	0.03	1.0	0.4

significant effects of maintained carnitine shuttle homeostasis, beneficial to mitochondrial integrity, were also observed. Consequently, an improved neural viability (i.e., higher NAA levels) corresponded with improved behavioral outcomes after kaempferol treatment. As a dietary flavonol compound, the safety of kaempferol has been well established in humans.[52] Further, kaempferol treatments improving TBI outcomes in the current study were within the dose limits demonstrated to be safe for humans. Because early-stage kaempferol treatment has demonstrated long-term benefits on brain functional and behavioral outcomes in the preclinical rat model of developmental TBI,[27] kaempferol based treatments can translate potentially to developmental age patients with TBI.

Acknowledgments

This study was supported by funding from the New Jersey Commission for Brain injury research (CBIR15IRG010; SK) and National Institutes of Health (R01NS097750; VS). Sample preparation and the LC/MS measurements were performed at the Proteomics and Metabolomics Core Facility at Weill Cornell Medicine, New York.

Author Disclosure Statement

No competing financial interests exist.

References

1. Biagi, L., Abbruzzese, A., Bianchi, M.C., Alsop, D.C., Del Guerra, A., and Tosetti, M. (2007). Age dependence of cerebral perfusion assessed by magnetic resonance continuous arterial spin labeling. J. Magn. Reson. Imaging 25, 696–702.
2. Chiron, C., Raynaud, C., Maziere, B., Zilbovicius, M., Laflamme, L., Masure, M.C., Dulac, O., Bourguignon, M., and Syrota, A. (1992). Changes in regional cerebral blood flow during brain maturation in children and adolescents. J. Nucl. Med. 33, 696–703.
3. Hales, P.W., Kawadler, J.M., Aylett, S.E., Kirkham, F.J., and Clark, C.A. (2014) Arterial spin labeling characterization of cerebral perfusion during normal maturation from late childhood into adulthood: normal 'reference range' values and their use in clinical studies. J. Cereb. Blood Flow Metab. 34, 776–784.
4. Chugani, H.T., Phelps, M.E., and Mazziotta, J.C. (1987) Positron emission tomography study of human brain functional development. Ann. Neurol. 22, 487–497.
5. Dobbing, J., and Sands, J. (1973) Quantitative growth and development of human brain. Arch. Dis. Child 48, 757–767.
6. Paus, T., Collins, D.L., Evans, A.C., Leonard, G., Pike, B., and Zijdenbos, A. (2001). Maturation of white matter in the human brain: a review of magnetic resonance studies. Brain Res. Bull. 54, 255–266.
7. Reiss, A.L., Abrams, M.T., Singer, H.S., Ross, J.L., and Denckla, M.B. (1996) Brain development, gender and IQ in children. A volumetric imaging study. Brain 119, 1763–1774.
8. Labarthe, D.R., Dai, S., Fulton, J.E., Harrist, R.B., Shah, S.M., and Eissa, M.A. (2009). Systolic and fourth- and fifth-phase diastolic blood pressure from ages 8 to 18 years: Project HeartBeat! Am. J. Prevent. Med. 37, S86–S96.
9. Winter, J.D., Dorner, S., Lukovic, J., Fisher, J.A., St Lawrence, K.S., and Kassner, A. (2011). Noninvasive MRI measures of microstructural and cerebrovascular changes during normal swine brain development. Pediatr. Res. 69, 418–424.
10. Greene, J.G., Greenamyre, J.T. (1996) Bioenergetics and glutamate excitotoxicity. Prog. Neurobiol. 48, 613–634.
11. Casey, P., McKenna, M., Saraswati, M., Robertson, C., and Fiskum, G. (2006) Traumatic brain injury in immature rats causes early and sustained alterations in cerebral metabolism. Crit. Care Med. 34, Suppl, A17.
12. Marino, S., Zei, E., Battaglini, M., Vittori, C., Buscalferri, A., Bramanti, P., Federico, A., and De Stefano, N. (2007). Acute metabolic brain changes following traumatic brain injury and their relevance to clinical severity and outcome. J. Neurol. Neurosurg. Psychiatry 78, 501–507.
13. Pascual, J.M., Solivera, J., Prieto, R., Barrios, L., Lopez-Larrubia, P., Cerdan, S., and Roda, J.M. (2007). Time course of early metabolic changes following diffuse traumatic brain injury in rats as detected by (1)H NMR spectroscopy. J. Neurotrauma 24, 944–959.
14. Robertson, C.L., Saraswati, M., Scafidi, S., Fiskum, G., Casey, P., and McKenna, M. (2013). Cerebral glucose metabolism in an immature rat model of pediatric traumatic brain injury. J. Neurotrauma 30, 2066–2072.
15. Viant, M.R., Lyeth, B.G., Miller, M.G., and Berman, R.F. (2005) An NMR metabolomic investigation of early metabolic disturbances following traumatic brain injury in a mammalian model. NMR Biomed. 18, 507–516.
16. Chitturi, J., Li, Y., Santhakumar, V., and Kannurpatti, S.S. (2018) Early behavioral and metabolomic change after mild to moderate traumatic brain injury in the developing brain. Neurochem. Int. 120, 75–86.
17. Lyons, D.N., Vekaria, H., Macheda, T., Bakshi, V., Powell, D.K., Gold, B.T., Lin, A.L., Sullivan, P.G., and Bachstetter, A.D. (2018). A mild traumatic brain injury in mice produces lasting deficits in brain metabolism. J. Neurotrauma 35, 2435–2447. 10.1089/neu.2018.5663
18. Lifshitz, J., Friberg, H., Neumar, R.W., Raghupathi, R., Welsh, F.A., Janmey, P., Saatman, K.E., Wieloch, T., Grady, M.S., and McIntosh, T.K (2003) Structural and functional damage sustained by mitochondria after traumatic brain injury in the rat: evidence for differentially sensitive populations in the cortex and hippocampus. J. Cereb. Blood flow Metab. 23, 219–231.
19. Kannurpatti, S.S. (2017) Mitochondrial calcium homeostasis: implications for neurovascular and neurometabolic coupling. J. Cereb. Blood Flow Metab. 37, 381–395.
20. Hosseini-Zare, M.S., Gu, F., Abdulla, A., Powell, S., and Ziburkus, J. (2017) Effects of experimental traumatic brain injury and impaired glutamate transport on cortical spreading depression. Exp. Neurol. 295, 155–161.
21. Fluegge, D., Moeller, L.M., Cichy, A., Gorin, M., Weth, A., Veitinger, S., Cainarca, S., Lohmer, S., Corazza, S., Neuhaus, E.M., Baumgartner, W., Spehr, J., and Spehr, M. (2012). Mitochondrial Ca(2+) mobilization is a key element in olfactory signaling. Nat. Neurosci. 15, 754–762.
22. Kannurpatti, S.S., Sanganahalli, B.G., Herman, P., and Hyder, F. (2015) Role of mitochondrial calcium uptake homeostasis in resting state fMRI brain networks. NMR Biomed. 28, 1579–1588.
23. Mathiesen, C., Caesar, K., Thomsen, K., Hoogland, T.M., Witgen, B.M., Brazhe, A., and Lauritzen, M. (2011). Activity-dependent increases in local oxygen consumption correlate with postsynaptic currents in the mouse cerebellum in vivo. J. Neurosci. 31, 18327–18337.
24. Sanganahalli, B.G., Herman, P., Hyder, F, and Kannurpatti, S.S. (2013) Mitochondrial calcium uptake capacity modulates neocortical excitability. J. Cereb. Blood Flow Metab. 33, 1115–1126.
25. Sanganahalli, B.G., Herman, P., Hyder, F., and Kannurpatti, S.S. (2013) Mitochondrial functional state impacts spontaneous neocortical activity and resting state FMRI. PLoS One 8, e63317,
26. Verweij, B.H., Muizelaar, J.P., Vinas, F.C., Peterson, P.L., Xiong, Y., and Lee, C P. (2000) Impaired cerebral mitochondrial function after traumatic brain injury in humans. J. Neurosurg. 93, 815–820.
27. Murugan, M., Santhakumar, V., and Kannurpatti, S. (2016) Facilitating mitochondrial calcium uptake improves activation-induced cerebral blood flow and behaviour after mTBI. Front. Syst. Neurosci. 10, 19.
28. Di Pietro, V., Amorini, A.M., Tavazzi, B., Vagnozzi, R., Logan, A., Lazzarino, G., Signoretti, S., Lazzarino, G., and Belli, A. (2014). The molecular mechanisms affecting N-acetylaspartate homeostasis following experimental graded traumatic brain injury. Mol. Med. 20, 147–157.
29. Moffett, J.R., Arun, P., Ariyannur, P.S., and Namboodiri, A.M. (2013) N-Acetylaspartate reductions in brain injury: impact on post-injury neuroenergetics, lipid synthesis, and protein acetylation. Front. Neuroenergetics 5, 11.
30. Gupta, A., Elgammal, F.S., Proddutur, A., Shah, S., and Santhakumar, V. (2012) Decrease in tonic inhibition contributes to increase in dentate semilunar granule cell excitability after brain injury. J. Neurosci. 32, 2523–2537.
31. Li, Y., Korgaonkar, A.A., Swietek, B., Wang, J., Elgammal, F.S., Elkabes, S., and Santhakumar, V. (2015). Toll-like receptor 4 en-

hancement of non-NMDA synaptic currents increases dentate excitability after brain injury. Neurobiol. Dis. 74, 240–253.
32. Xia, J., Sinelnikov, I.V., Han, B., and Wishart, D.S. (2015) MetaboAnalyst 3.0–making metabolomics more meaningful. Nucleic acids research 43, W251–W257.
33. Xia, J., Psychogios, N., Young, N., and Wishart, D.S. (2009) MetaboAnalyst: a web server for metabolomic data analysis and interpretation. Nucleic Acids Res. 37, W652–W660.
34. Tang, L., Peng, S., Bi, Y., Shan, P., and Hu, X. (2014) A new method combining LDA and PLS for dimension reduction. PLoS One 9, e96944.
35. Xia, J., and Wishart, D.S. (2010) MetPA: a web-based metabolomics tool for pathway analysis and visualization. Bioinformatics 26, 2342–2344.
36. Xia, J., and Wishart, D.S. (2010) MSEA: a web-based tool to identify biologically meaningful patterns in quantitative metabolomic data. Nucleic Acids Res. 38, W71–W77.
37. Schallert, T., Fleming, S.M., Leasure, J.L., Tillerson, J.L., and Bland, S.T. (2000) CNS plasticity and assessment of forelimb sensorimotor outcome in unilateral rat models of stroke, cortical ablation, parkinsonism and spinal cord injury. Neuropharmacology 39, 777–787.
38. Parent, M., Li, Y., Santhakumar, V., Hyder, F., Sanganahalli, B.G., and Kannurpatti, S.S. (2018). Alterations of parenchymal microstructure, neuronal connectivity, and cerebrovascular resistance at adolescence after mild-to-moderate traumatic brain injury in early development. J. Neurotrauma. Epub ahead of print.
39. Di Giorgio, A.M. Hoy, Y., Zhao, X., Zhang, B., Lyeth, B.G., and Russell, M.J. (2008) Dimethyl sulfoxide provides neuroprotection in a traumatic brain injury model. Restor. Neurol. Neurosci. 26, 501–507.
40. Len, T.K., and Neary, J.P. (2011) Cerebrovascular pathophysiology following mild traumatic brain injury. Clin. Physiol. Funct. Imaging 31, 85–93.
41. Lifshitz, J., Lisembee, A.M. (2011) Neurodegeneration in the somatosensory cortex after experimental diffuse brain injury. Brain Struct. Funct. 217, 49–61.
42. Povlishock, J.T., and Christman, C.W. (1995) The pathobiology of traumatically induced axonal injury in animals and humans: a review of current thoughts. J. Neurotrauma 12, 555–564.
43. Kelley, B.J., Lifshitz, J., and Povlishock, J.T. (2007) Neuroinflammatory responses after experimental diffuse traumatic brain injury. J. Neuropathol. Exp. Neurol. 66, 989–1001.
44. Park, E., Bell, J.D., and Baker, A.J. (2008) Traumatic brain injury: can the consequences be stopped? CMAJ 178, 1163–1170.
45. Putatunda, R., Bethea, J.R., and Hu, W.H. (2018) Potential immunotherapies for traumatic brain and spinal cord injury. Chin. J. Traumatol. 21, 125–136.
46. Ferreira, G.C., and McKenna, M.C. (2017) L-Carnitine and acetyl-L-carnitine roles and neuroprotection in developing brain. Neurochem. Res. 42, 1661–1675.
47. Scafidi, S., Fiskum, G., Lindauer, S.L., Bamford P., Shi, D., Hopkins, I., and McKenna. M.C. (2010). Metabolism of acetyl-L-carnitine for energy and neurotransmitter synthesis in the immature rat brain. J. Neurochem. 114, 820–831.
48. Jones, L.L., McDonald, D.A., and Borum, P.R. (2010) Acylcarnitines: role in brain. Prog. Lipid Res. 49, 61–75.
49. Scafidi, S., Racz, J., Hazelton, J., McKenna, M.C., and Fiskum, G. (2010) Neuroprotection by acetyl-L-carnitine after traumatic injury to the immature rat brain. Dev. Neurosci. 32, 480–487.
50. Montero, M., Lobaton, C.D., Hernandez-Sanmiguel, E., Santodomingo, J., Vay, L., Moreno, A., and Alvarez, J. (2004). Direct activation of the mitochondrial calcium uniporter by natural plant flavonoids. Biochem. J. 384, 19–24.
51. Vay, L., Hernandez-Sanmiguel, E., Santo-Domingo, J., Lobaton, C D., Moreno, A., Montero, M., and Alvarez, J. (2007). Modulation of Ca(2+) release and Ca(2+) oscillations in HeLa cells and fibroblasts by mitochondrial Ca(2+) uniporter stimulation. J. Physiol. 580, 39–49.
52. DuPont, M.S., Day, A.J., Bennett, R.N., Mellon, F.A., and Kroon, P.A. (2004) Absorption of kaempferol from endive, a source of kaempferol-3-glucuronide, in humans. Eur. J. Clin. Nutr. 58, 947–954.

Address correspondence to:
Sridhar S. Kannurpatti, PhD
Department of Radiology
Rutgers Biomedical and Health Sciences
New Jersey Medical School
ADMC5, Room 575
30 Bergen Street
Newark, NJ 07101

E-mail: kannursr@njms.rutgers.edu